International Journal of All Research Education and Scientific Methods (IJARESM), ISSN: 2455-6211
Volume 9, Issue 3, March -2021, Impact Factor: 7.429, Available online at: www.ijaresm.com

Electrical and Magnetic Properties of $Cd_{1-X}Fe_{2-X}Co_xBi_{0.3}O_4$ Nanoparticles Synthesized by Chemical Co-precipitation Technique

G. S. Gugale[1], V. U. Pandit[2], D. V. Nighot[3], R. A. Pawar[4], V. S. Jawale[5], M. B. Khanwilkar[6], A. K. Nikumbh[7]

[1,2]Department of Chemistry, Haribhai V. Desai College, Pune- 411 002 (India)
[3]Department of Engineering Sciences, AISSMS, College of Engineering, Pune, 411 001, India
[4,5]Prof. Ramkrishna More College, Akurdi, Pune 411044, India
[6]Department of Chemistry, K.M.C. College, Khopoli, Dist. Raigad, Khopoli, 410203, India
[7]Department of Chemistry, Savitribai Phule Pune University, Pune, India

----------**********----------

ABSTARCT

The nanoparticles of $Cd_{1-x}Fe_{2-x}Co_xBi_{0.3}O_4$ ferrites (x = 0.0 - 2.0) were prepared by the tartarate coprecipitation technique. The formation of the ferrite phase was confirmed by X- ray diffraction, which is a characteristic of the spinel ferrite. Increase in lattice constant was observed with increase in x. These samples showed the usual temperature dependence electrical conductivity having the ferrimagnetic to paramagnetic transitions. The magnetic properties such as the saturation magnetization (Ms), coercivity (Hc) and ratio of remanences to saturation magnetization (MR/MS) were obtained from the hysteresis loop. It is observed that the Ms and Hc increases with increase of x, which is attributed to the presence of an ultration layer at the grain boundaries that impedes the domain wall motion. The observed low magnetic moment can be explained in forms of spin canting at the surface of nanoparticles. The electrical and magnetic properties suggest that, both N'eels two sublattice and Yafet - Kittel models exist for x = 0.4 to 0.8. The increase in coercivity suggests that the material can be used for applications in perpendicular recording media.

Keywords: Ferrites, Spinal, Ferrimagnetic, Co-precepetation, Magnetic

INTRODUCTION

Ferrites are the ferrimagnetic mixed oxides having the general formula MFe_2O_4, where M is a divalent metal ion such as Mg, Mn, Zn, Ni, Co, Fe, Cd and Cu. Owing to their important electrical and magnetic properties, ferrites are extensively used in electronic industry. It is well known that the intrinsic properties of ferrites depend on the chemical composition, preparative conditions and substitutions **[1]**. By introduction of a relatively small amount of foreign ion, important modifications in structural and magnetic properties can be obtained **[2, 3]**.

Magnetic behaviour of mixed Cd - Co ferrites has been studied by many authours **[4-15].** The substitution of Fe^{3+} by Al^{3+}, Cr^{3+} and Gd^{3+} for this system have been reported **[16-19]**. The effect of rare - earth (Sm, Gd, La, Nd and Dy) substitution on electrical properties of Cu-Zn ferrites have been extensively studied **[20, 21]**. Rezlescu *et. al* **[1]** had reported the effect of rare - earth (Yb, Er, Dy, Er, Gd, Sm, Ce) substitution on magnetization and initial permeability in Ni - Zn ferrite system. Influence of Nd^{3+} substitution on magnetization and initial permeability in Zn-Mg ferrite system have also been studied **[22]**.

It is known that the magnetic behaviour of the ferrimagnetic oxide compounds is largely governed by the Fe-Fe interaction (the coupling of the spins of the 3d electrons). By introducing Dy^{3+} or Bi^{3+} ions in the spinel lattice, the Bi-Fe interactions appear too, which can lead to small changes in the magnetization and Curie temperature.

In this paper we present some results concerning the influence of Bi^{3+} ions substituting the iron ions in the $Cd_{1-x}Co_xFe_{1.7}Bi_{0.3}O_4$ ferrite on its structural, electrical and magnetization properties of the system. This nano system may useful for formation of composites with other organic and inorganic materials for hydrogen generation and dye degradation **[23-28]**.

EXPERIMENTAL

The tartarate precursors ($CdFe_{1.7}Bi_{0.3}$ $(C_4H_4O_6)_3{\cdot}H_2O$ and $CoFe_{1.7}Bi_{0.3}$ $(C_4H_4O_6)_3{\cdot}0.5H_2O$) and a series of mixed ferritspinels $Cd_{1-x}Co_xFe_{1.7}Bi_{0.3}O_4$ (where $0 \le x \le 1$) were synthesized using co-precepetation method as follows,

Synthesis of Cobalt - iron - bismuth tartarate half hydrate $CoFe_{1.7}Bi_{0.3}(C_4H_4O_6)_3 \cdot 0.5H_2O$

A mixture of $CoSO_4 \cdot 7H_2O$ (5.009 gm), $FeSO_4 \cdot 7H_2O$ (8.428 gm) and $Bi(NO_3)_3 \cdot 5H_2O$ (2.593 gm dissolved in dilute HNO_3) were used. The sodium tartarate solution was added slowly with constant stirring till a permanent precipitate was occurred. The light brown coloured precipitate was obtained. The precipitate was filtered and washed with distilled water and air dried at ambient temperature. Yield =13.95 gm.

Cadmium - cobalt - iron - bismuth tartarates, $Cd_{1-x}Co_xFe_{1.7}Bi_{0.3}(C_4H_4O_6)_3 \cdot nH_2O$

A mixture of $3CdSO_4 \cdot 8H_2O$ (3.137 to 0.784 gm), $CoSO_4 \cdot 7H_2O$ (1.002 to 4.007gm), $FeSO_4 \cdot 7H_2O$ (7.466 to 8.187 gm) and $Bi(NO_3)_3.5H_2O$ (2.298 to 2.519 gm in dilute HNO_3) were dissolved in 100ml deionized water. The concentration of cadmium and cobalt were adjusted in the weight percent range x = 0.2 to 0.8. To this 10% sodium tartarate solution was added, till a permanent precipitate occurred.

(The flowshit diagram for tartarate precursors and subsequent conversion to ferrites is shown below).
Solutions of cadmium sulphate, ferrous sulphate, cobalt sulphate and bismuth nitrate were mixed together in a beaker. To the above solution dilute sulphuric acid is added to make pH slightly acidic. Above clear solution is continuously stirred on a magnetic stirrer and maintained temperature to 50°C. To this clear solution 10% sodium tartarate is added and resultant precepetate stirred vighrously for 30 min. Precepetation filtered and washed with water and acetone and dried at 80°C. This powder is calcined at 800°C for 2 hrs. in static air atmosphere. The resultant material is subjected for the chemical analysis, X- ray diffraction pattern, infrared spectroscopy, electrical conductivity, thermoelectric power, magnetic hysteresis and initial magnetic susceptibility. **[29]**

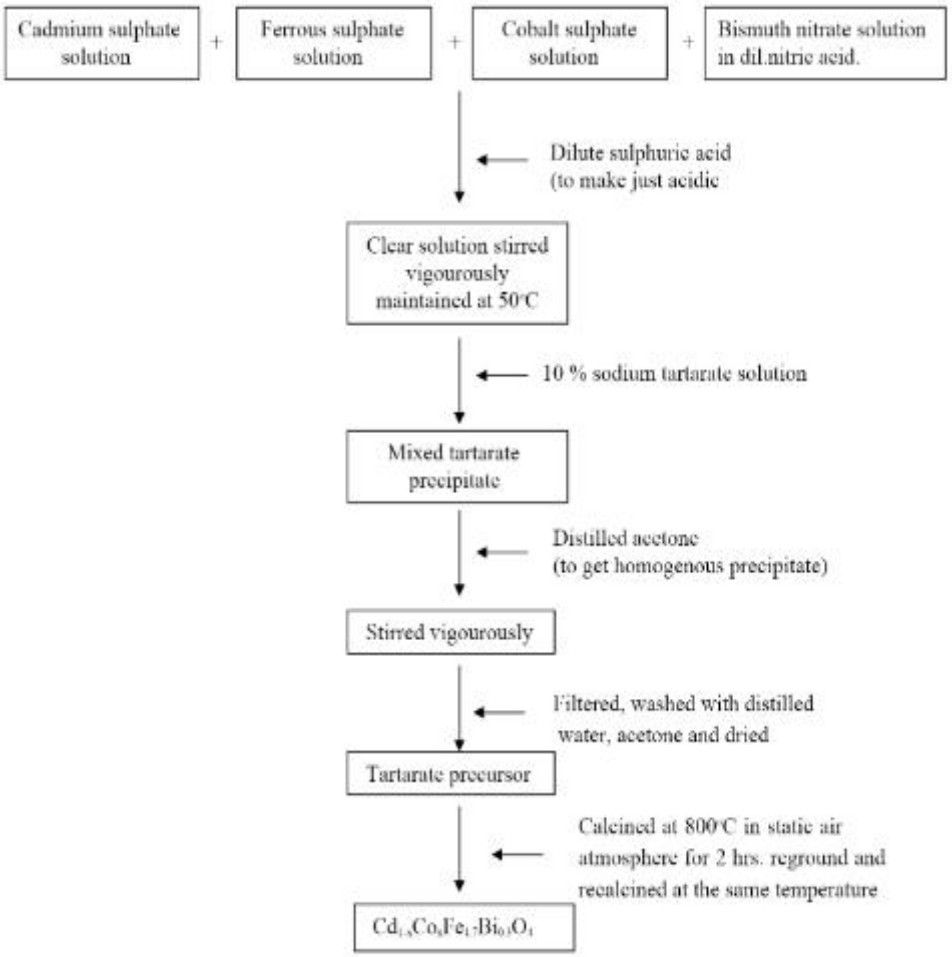

The experimental set up including furnace was fabricated in our laboratory. The sample holder assembly and the furnace used in these experiments for high temperature resistance measurements was constructed by winding a standard resistor Kanthol wire (65 Ohms) on a ceramic tube of 3cm inner diameter and length of 30cm, so as to obtain a constant temperature zone of about 15cm in length at the centre of the furnace. This assembly was fixed in aluminum box by asbestos powder and plaster of paris in order to avoid heat transfer. The temperature of furnace could be controlled (±1°C) by making use of variac and suitable voltage stabilizer.

About 1 g of compound was thoroughly powdered in a agate mortar for 10 minutes and pressed in a die of 10 mm diameter by a hydraulic press (Sushank Ltd., India) assembled at Central Workship, University of Pune, fitted with a calibrated pressure gauge. The pressure was released after 1 minute and the pellet was removed by applying the pressure in the opposite direction. The pellet thus obtained was 3.5 ± 0.02 mm in thickness.

The pellet of 10 mm diameter and about 3.5 ± 0.02 mm in thickness was pressed between the platinum discs (15 mm diameter and 0.5 mm thickness) fixed at the ends of two graphite rods; one of these graphite rods was spring loaded to obtain good pressure contact. The platinum wires fused to the platinum foils were insulated by porcelain beads, and were taken out for connections. A mica sheet was put in between the platinum discs and fixed graphite rods for insulation. The sample was placed in the constant temperature zone of a tubular furnace. The temperature of the furnace could be maintained within ± 1°C as a desired value by means of an automatic controller (Philips plastomatic). Two pre-calibrated chromel-alumel thermocouples were placed very near the two ends of the samples to sense the temperature (± 1°C) at both ends.

The resistance of the sample was measured by the current - voltage method. The sample was connected in series with a standard resistance and a d. c. power supply (Eveready Battery, 9.0V) was used. The voltage V_1 and V_2 developed across the sample and the standard resistances were read directly on a sensitive D.C. micro-voltmeter (Philips PP-9004). The temperature of the sample (i.e. the thermocouple voltage) and the sample voltage were measured using a same micro-voltmeter.

For the measurement of electrical conductivity in nitrogen atmosphere, pure and dry nitrogen was passed through the above assembly (pure nitrogen obtained from nitrogen cylinder of Indian Oxygen Company was passed through empty trap, then through concentrated sulphuric acid for removing moisture, and then through alkaline pyrogallol for removing traces of oxygen and finally through a trap containing sodium hydroxide pellets with dry adsorbent cotton to get almost 99.8% pure nitrogen). The measurements were carried out keeping a slow continuous flow of nitrogen gas.

The temperature variation of electrical conductivity samples in a pellet form was determined in static air, dynamic nitrogen, dynamic air and dynamic air with water vapour. For dynamic air, an air compressor was used. The flow was maintained between 65 to 70 ml min^{-1}. For the decomposition study, the heating rate of about 5°C per minute was manually controlled with a predetermined operation of the variac. The precautions were taken to keep the rate of heating constant.

The measurements of Hall coefficient and thermoelectric power (i.e.Seebeck voltage) are useful to determine the sign and number of the charge carriers in a semiconductor. The thermoelectric power is the ratio of the gradient in temperature when the latter becomes small. Since magnetic oxides are high resitivity materials, a measurement of thermoelectric power is performed in the present work.

When temperature gradient is imposed across the ends of a sample, the charge carriers at the hot end will have a large velocity component along the direction of diminishing temperature than do the carriers at the cold end. Consequently, there occurs a net movement of the charge carriers such that an excess of carriers accumulates at the cold end and a deficiency of carriers is developed at the hot end. This produces a gradient in the electrochemical potential across the sample.

In the present work the integral method for the measurements of thermoelectric power was used. In this method, the two ends of the sample were maintained at the different temperatures T_1 and T_2. A thermoelectric potential difference was then produced along the sample. The voltage drop across the sample was measured by a null method across two contact junctions of the sample. The sign of the majority charge carriers could be deduced from the sign at cold end. A positive sign of the cold end indicated that the sample was p - type and a negative sign of cold end indicated that the sample was n - type semiconductor.

The sample in the form of a pellet of 10 mm thickness was pressed between two platinum discs fixed at the ends of two graphite rods. During the measurements, the sample was equilibrated at each temperature for about 15 minutes. The temperature differences of 2 - 20°C were used along the sample. The thermoelectric voltage (i.e.Seebeck voltage) developed across the sample and the temperature of the sample ends were read on Philips PP 9004 microvoltmeter. A set of values of thermoelectric voltage at various temperatures thus obtained (μ volts K^{-1}) was plotted against the respective absolute temperature. The sign of the probes at the lower temperature was the sign of Seebeck voltage

RESULTS AND DISCUSSION

Characterization

The chemical analysis was done using a Perkin - Elmer model 3100 Atomic Absorption Spectrometer (AAS) employing an air acetylene flame and a hallow cathode lamp as the light source. The duplicate samples (known amount of tartarate precursors dissolved in 2ml concentrated HCl and 5ml HNO_3. The final volume was made to 100ml) were

used for this analysis. A separate lamp was used for the dermination of each element. A blank solution (distilled water) was run before and after the aspiration of every sample into flame.

The infrared spectra of precursor were recorded in the region 4000 - 450 cm^{-1} on the Perkin - Elmer 783 spectrophotometer using nujol mull. Similarly, infrared spectra of magnetic and superconducting oxides were recorded in the region 700 - 200 cm^{-1} on the Perkin - Elmer spectrum - 2000, using KBr discs.

Thermal decomposition of precursors was recorded on Mettler TA 4000 instruments. Simultaneous thermogravimetric analysis (TGA), derivative thermogravimetry (DTG) and differential thermal analysis (DTA) were done under static air, dynamic air and dynamic dry nitrogen atmosphere. All the experiments were carried out under the identical conditions. Sample weight ~ 5 mg : Sample holder - platinum crucible, temperature 30 to 900°C, heating rate 5°C min^{-1}.

The X-ray powder diffraction patterns were determined on RegakuMiniflex diffractometer using CuKα radiation (λ = 1.5405 A°; nickel filter). The structural analysis magnetic and superconducting oxides were done by comparing the experimental d values and relative intensities with ASTM powder file. The d values were calculated using the following Bragg's equation ($n\lambda = 2d \sin\theta$).

Characterization of precursor

The chemical analysis of $CdFe_{1.7}Bi_{0.3}(C_4H_4O_6)_3 \cdot H_2O$ and $CoFe_{1.7}Bi_{0.3}(C_4H_4O_6)_3 \cdot 0.5H_2O$ are presented in Table I and it is in good agreement with the calculated values. The thermal analysis measurements confirm the presence of the water of hydration of these precursors. All compounds synthesized are paramagnetic at room temperature (Table II). These values are smaller than those obtained by summing up the magnetic moments of the metal ions. This indicates an antiferromagnetic interaction, generally present in such dicarboxylate coordination compounds. Thermal decomposition of these precursors shows the dehydration and decomposition in the temperature range 50-390^{0}C. It is observed that the weight loss in TGA corresponds to the formation of respective ferrites.

Table I: Observed chemical analysis of $Cd_{1-x}Co_xFe_{1.7}Bi_{0.3}O_4$

Compound	Wt. % of (± 0.5)							
	Cd		Co		Fe		Bi	
	Req.	Found	Req.	Found	Req.	Found	Req.	Found
$CdFe_{1.7}Bi_{0.3}O_4$	33.65	34.12	---	---	28.42	28.93	18.77	18.14
$Cd_{0.8}Co_{0.2}Fe_{1.7}Bi_{0.3}O_4$	27.81	28.23	3.64	3.28	29.36	28.82	19.33	19.63
$Cd_{0.6}Co_{0.4}Fe_{1.7}Bi_{0.3}O_4$	21.75	21.03	7.54	6.98	30.36	29.83	20.05	21.92
$Cd_{0.4}Co_{0.6}Fe_{1.7}Bi_{0.3}O_4$	14.89	15.11	11.71	12.08	31.44	31.85	20.76	21.13
$Cd_{0.2}Co_{0.8}Fe_{1.7}Bi_{0.3}O_4$	7.72	8.83	16.15	15.81	32.59	31.87	21.25	20.76
$CoFe_{1.7}Bi_{0.3}O_4$	---	---	21.00	20.88	33.84	34.02	22.35	21.77

Charaterization of Bi^{3+} substituted Cd - Co ferrites

Compositional Analysis

The composition of $Cd_{1-x}Co_xFe_{1.7}Bi_{0.3}O_4$ samples were determined by atomic absorption spectroscopy (AAS). The observed compositions are summerized in Table I. The proportion of ingredient elements showed that the weight proportions were correct in the final product. This suggests that the stoichiometry in the compounds is perfectly maintained i.e. $(Cd_{1-x}Co_x)$: Fe ratio is 1: 2 within the experimental error (< 1%).

X-ray diffraction studies

The X-ray diffraction patterns of $Cd_{1-x}Co_xFe_{1.7}Bi_{0.3}O_4$ ($0 \le x \le 1$) are shown in Figure 1. For all the samples of these ferrites, there are no ambiguous reflections in the diffractograms exhibiting the formation of single - phase with cubic structure compounds. The experimentally observed d - spacing values and relative intensities were compared with those reported in literature. The lattice parameter for each composition was then calculated and shown in Table III. It shows that the lattice parameter decreases linearly with the increase of cobalt content. Our results are explained on the assumption that substituting cobalt ions instead of cadmium ions in the composition caused the movement of Fe^{3+} ions from the octahedral (B) site and tetrahedral (A) site. The decrease in lattice constant is also due to the replacement of the smaller Fe^{3+} ion in the octahedral site by comparatively larger Co^{2+} ions i.e. Fe^{3+} has an ionic radius of 0.63 A° and Co^{2+} has an ionic radius of 0.72 A°. In other words replacement of larger Cd^{2+} (ionic radius = 0.97 A°) by

comparatively smaller Fe^{3+} in tetrahedral site. However, on substitution of Bi^{3+} no significant change in lattice constant was observed, which may be due to comparable ionic volumes of Cd^{2+} and further because the amount of Bi^{3+} per formula unit is rather small. Similar results have been reported in literature **[1, 9,]** for bismuth substituted Ni - Zn and Cu - Cd ferrite system suggesting occupancy of bismuth on octahedral (B) site.

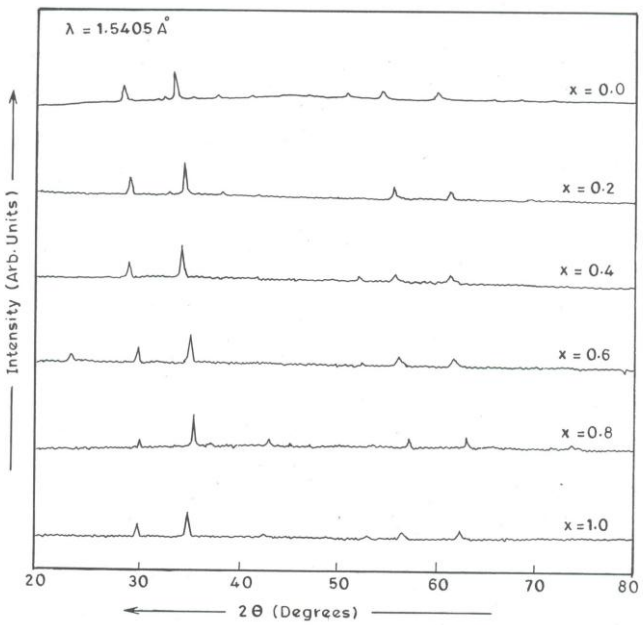

Fig. 1: X-ray powder diffraction pattern of $Cd_{1-x}Co_xFe_{1.7}Bi_{0.3}O_4$ system ($0 \leq x \leq 1$).

The crystelline sizes of these samples were calculated from the full width at - half maximum of (620), (440), (511), (422), (400), (311) and (220) diffraction peaks using Debye - Scherrer formula**.** The mean values of the crystallite diameters < D >x-ray are given in Table III. As can be seen from Table, the mean crystallite sizes are in the range of 21.568 to 30.031 nm.

The parculate properties like X-ray density (Dx), apparent density (D) and porosity (P) of $Cd_{1-x}Co_xFe_{1.7}Bi_{0.3}O_4$ samples are summarized in Table III. It is noticed that the X-ray densities for all composition of Cd-Co ferrites decreases with cobalt addition. The X-ray densities, Dx, are higher than the apparent densities, D. This is attributed to the existence of the pores which depends on the sintering conditions. The porosity increases with cobalt content, and higher porosity corresponds with lower apparent density, D (Table III). The results are explained on the basis that Co^{2+} has a smaller atomic weight and smaller atomic radius than Cd^{2+}. The substitution of cobalt ions into the lattice instead of cadmium gives a lower density, which leads to increase of porosity.

Table III: X-ray powder diffraction data for $Cd_1Co_xFe_{1.7}Bi_{0.3}O_4$

Compound	Lattice parameter (nm)	Mean Crystalline Size (nm)	X-ray Density (gcm^{-3})	Apparent density (gcm^{-3})	Porosity P=1-D/Dx
$CdFe_{1.7}Bi_{0.3}O_4$	0.868	26.364	6.775	1.860	0.725
$Cd_{0.8}Co_{0.2}Fe_{1.7}Bi_{0.3}O_4$	0.861	27.494	6.721	1.747	0.740
$Cd_{0.6}Co_{0.4}Fe_{1.7}Bi_{0.3}O_4$	0.855	24.420	6.638	1.533	0.769
$Cd_{0.4}Co_{0.6}Fe_{1.7}Bi_{0.3}O_4$	0.842	28.790	6.711	1.493	0.777
$Cd_{0.2}Co_{0.8}Fe_{1.7}Bi_{0.3}O_4$	0.841	30.031	6.590	1.328	0.796
$CoFe_{1.7}Bi_{0.3}O_4$	0.839	24.155	6.295	1.203	0.809

Infrared spectral studies

Infrared spectra of $Cd_{1-x}Co_xFe_{1.7}Bi_{0.3}O_4$ samples (Table IV) show two strong bands ν_1 and ν_2 in the frequency range 400 cm^{-1} to 700 cm^{-1}. The absence of the low frequency bands in our compounds suggest that the lattice vibrations which are

responsible for these bands are very weak. The band positions are listed in Table IV. It can be easily noticed that no shift occurs in the position of bands at frequency ν_2 by increasing the cobalt content. Also, it can be seen that the frequency ν_1 for $CdFe_{1.7}Bi_{0.3}O_4$ (normal spinel) is shifted to higher frequencies with incresing cobalt ion concentration and changes to $CoFe_{1.7}Bi_{0.3}O_4$ (inverse spinel). In an inverse spinel, the octahedral site is occupied by Fe^{3+} and the divalent ion Co^{2+}. Due to charge imbalance the oxygen ion is likely to shift towards the Fe^{3+} ion making the force constant between Fe^{3+} and O^{2-} more. Hence, we expect an increase in bond stretching mode, frequencies as we go from normal to inverse spinel. Therefore, we find that ν_1 increases as x is increased and ν_2 do not change with the type of spinel structure, given in Table IV.

Table IV: Infrared spectral data for $Cd_{1-x}Co_xFe_{1.7}Bi_{0.3}O_4$

Compound $CdFe_{1.7}Bi_{0.3}O_4$	Infrared Spectral absorption band (cm^{-1})	
	ν_1	ν_1 458
$CdFe_{1.7}Bi_{0.3}O_4$	545	458
$Cd_{0.8}Co_{0.2}Fe_{1.7}Bi_{0.3}O_4$	554	460
$Cd_{0.6}Co_{0.4}Fe_{1.7}Bi_{0.3}O_4$	560	461
$Cd_{0.4}Co_{0.6}Fe_{1.7}Bi_{0.3}O_4$	571	460
$Cd_{0.2}Co_{0.8}Fe_{1.7}Bi_{0.3}O_4$	584	459
$CoFe_{1.7}Bi_{0.3}O_4$	580	457

Electrical conductivity studies

Figure 2 shows the log σ against T^{-1} heating plots of $Cd_{1-x}Co_xFe_{1.7}Bi_{0.3}O_4$ samples. The experiments were repeated several times and the results were always found to be reproducible. The room temperature conductivity values σ_{RT} for all the compounds of these systems were found to vary between 10^{-9} and 10^{-12} Ω^{-1} cm^{-1}, for different values of x. Therefore, these samples are semi-conducting in nature.

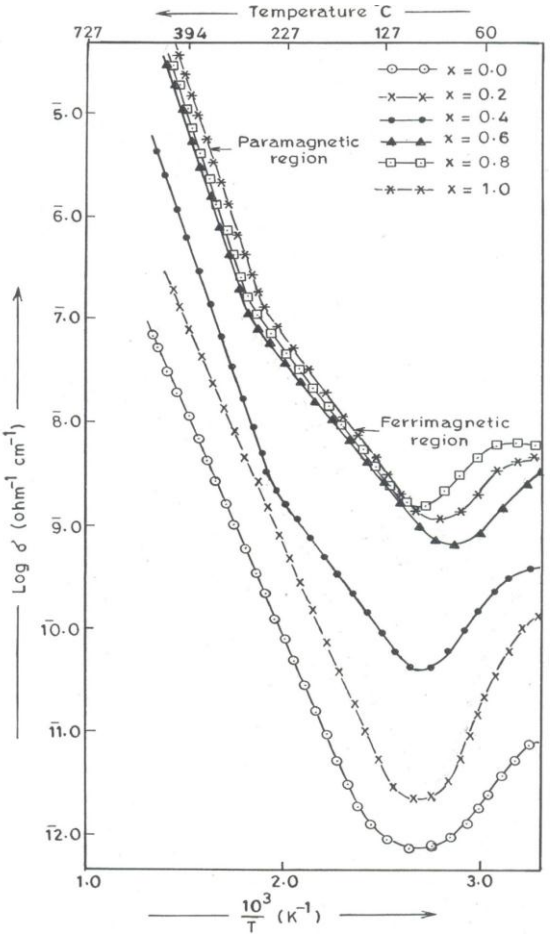

Fig. 2: Plot of log σ against T^{-1} of For $Cd_{1-x}Co_xFe_{1.7}Bi_{0.3}O_4$ systems ($0 \leq x \leq 1$).

The log σ against T^{-1} for all composition shows (Fig.2) a decrease in electrical conductivity in the temperature range 313 to 388 K. The σ values are then increases showing a definite kink (brake) at about 500 to 563 K except for $Cd_{0.8}Fe_{1.7}Bi_{0.3}O_4$ and $Cd_{0.8}Co_{0.2}Fe_{1.7}Bi_{0.3}O_4$, on further increase of temperature, the σ value increases as temperature increases. The decrease in conductivity in the temperature around 388 K (Table II) corresponds to desorption of adsorbed water molecules, usually adsorbed water molecules behave as an electron donor. The kink occurs in each curve, at temperature (see Table II) which corresponds to ferrimagnetic to paramagnetic transition. The kink will be most marked for those cases (i.e., $x \geq 0.2$) in which there are a strong exchange interaction between the outer and inner electrons.

Table II: D.C. electrical conductivity data of $Cd_{1-x}Co_xFe_{1.7}Bi_{0.3}O_4$ systems ($0 \leq x \leq 1$)

Compounds	Temperature corresponding to desorption of adsorbed water (K)	σ at 525 K $\Omega^{-1}cm^{-1}$	Activation energy Ea (eV)	
			Ferrimagnetic	Paramagnetic
$CdFe_{1.7}Bi_{0.3}O_4$	373	2.14×10^{-10}	---	0.875
$Cd_{0.8}Co_{0.2}Fe_{1.7}Bi_{0.3}O_4$	370	1.84×10^{-9}	---	0.853
$Cd_{0.6}Co_{0.4}Fe_{1.7}Bi_{0.3}O_4$	370	2.92×10^{-9}	0.471	1.093
$Cd_{0.4}Co_{0.6}Fe_{1.7}Bi_{0.3}O_4$	350	1.25×10^{-7}	0.494	1.141
$Cd_{0.2}Co_{0.8}Fe_{1.7}Bi_{0.3}O_4$	370	1.72×10^{-7}	0.499	1.163
$CoFe_{1.7}Bi_{0.3}O_4$	360	1.37×10^{-7}	0.528	1.179

The two activation energies are calculated for the two regions around the kink points, firstly for ferrimagnetic and secondly for paramagnetic region. The observed values of the activation energies, E_a (eV), for the series $Cd_{1-x}Co_xFe_{1.7}Bi_{0.3}O_4$ are listed in Table II. The values of activation energies, Ea (eV), in the paramagnetic region is higher than that in the ferrimagnetic region. The behaviour of the activation energy on passing through break point may be explained by the double exchange mechanism. Hence, the conduction of Bi^{3+} substituted Cd - Co ferrite system is due to the electron hopping in the sublattices between $Fe^{2+} \leftrightarrow Fe^{3+}$ ions and results increasing in activation energy in the paramagnetic region. It can also be seen that the conductivity increasing with the increase of cobalt concentration (Table II). This may be due to the presence of a large number of cobalt ions (which can show the Co^{2+} to Co^{3+} mechanism) in the sample.

In our samples Cd^{2+} ions have a preference for A sites only, and therefore they cannot play a role in affecting Ea values in Bi^{3+} substituted Cd - Co ferrites. Thus, the increase in Ea can be attributed to Bi^{3+} occupying octahedral B - sites, which are also confirmed by infrared spectroscopy. Another reason is that, as the cobalt concentration (x) increases in $Cd_{1-x}Co_xFe_{1.7}Bi_{0.3}O_4$ spinels, the antiferromagnetic order changes and enhances the activation energy for electrical conduction. Therefore, the magnetic ordering changes might be responsible for the increase in the activation energy. Hopping between ions of different metals on the octahedral sublattices needs higher activation energy than for ions of the same metal. Thus, conduction activation energy for x = 1.0 is higher.

Further, for such spinel compounds, the A - A and A - B distances are longer than B - B distances for the respective metal ions, suggesting that B - site cations are responsible for the conduction in these compounds, since exchange of electrons would be favoured. In our samples, however, on the substitution of Bi^{3+}, the conductivity of material is increased, indicating that although Bi^{3+} takes the octahedral B - sites, it impedes the conduction mechanism. This means that the electron transfer that takes place between Fe^{3+} to Fe^{2+} is not favoured in the case of Fe^{3+} and Bi^{3+}, thus suggesting that Bi^{3+} does not take part in conduction mechanism.

Thermoelectric power measurements

The thermoelectric power measurements for $Cd_{1-x}Co_xFe_{1.7}Bi_{0.3}O_4$ in Fig.3 shows an initial fall in the number of charge carriers (negative charge carriers) in the temperature range up to 460 K and beyond this temperature the number increases up to 650 K and then slowly decreases as temperature increases. The common feature for all the compositions is that, the thermoelectric power is negative over the whole range of temperature, indicating that the charge carriers are electrons (i.e., n - type). Initial decrease in the number of charge carriers is due to desorption of adsorbed water molecule. It increases in magnitude with temperature in the paramagnetic region. This might be due to hopping of electrons from Fe^{2+} to Fe^{3+} ions.

International Journal of All Research Education and Scientific Methods (IJARESM), ISSN: 2455-6211
Volume 9, Issue 3, March -2021, Impact Factor: 7.429, Available online at: www.ijaresm.com

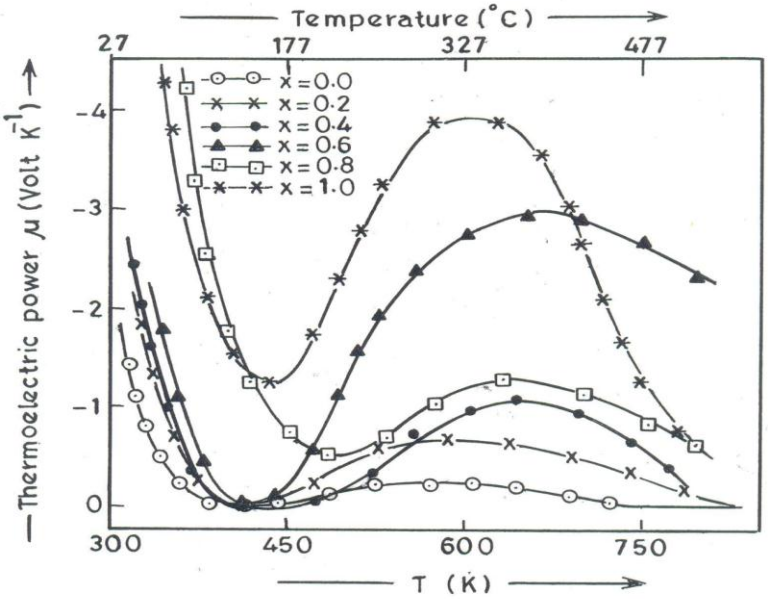

Fig. 3: Plot of thermoelectric power, μ (volt K^{-1}) against T^{-1} (K) of For $Cd_{1-x}Co_xFe_{1.7}Bi_{0.3}O_4$ systems ($0 \leq x \leq 1$).

The observed low value of thermoelectric power could be explained on the basis of the substitution of Bi^{3+} ions which occupy octahedral (B) sites, which leads to replacement of Fe^{3+} ions from B - sites. The Bi^{3+} ions reduce the number of Fe^{3+} ions where part of them reduces to Fe^{2+} during the sintering process, so the negative thermoelectric power i.e. n - type conduction mechanism would be lower. Thus it is assumed that in $Cd_{1-x}Co_xFe_{1.7}Bi_{0.3}O_4$ systems, the carriers are created by the following reaction of the electron exchange on the octahedral sites of the spinel lattice:

$$Co^{2+} + Fe^{3+} \quad \rightleftharpoons \quad Co^{3+} + Fe^{2+}$$

The pairs Co^{2+} - Fe^{3+} may be regarded as donors.

Magnetic studies

The Bi^{3+} substituted with $x \geq 0.2$ of Cd - Co ferrites showed a definite hysteresis loop at room temperature, which indicates the ferrimagnetic behaviour. From the hysteresis loops, the coercive force (H_C), saturation magnetization (M_S), ratio of remanance to saturation magnetization (M_R/M_S), magnetic moment (n_B) and YK angles (θ_{YK}) values have been listed in Table V. The compound with x = 0.00 for $Cd_{1-x}Co_xFe_{1.7}Bi_{0.3}O_4$ does not show hysteresis loop, therefore we did not observe any magnetization for these samples at room temperature, since these compounds are antiferromagnetic in nature.

From Table V, it is seen that as the content of cobalt is increased, the value of M_S also increases up to x = 0.6, beyond which a decreasing trend is exhibited. The variation of magnetization of such samples ($x \geq 0.2$) can be explained on Nèel two sublattice models of ferrimagnetism**.** The introduction of cobalt ions which have a strong preference for the spinel at B - site and the cation distribution is given by,

$$(Cd^{2+}_{1-x}\ Fe^{3+}_{x})\ [Fe^{3+}_{1.7-x}Co^{2+}_{x}M^{3+}_{0.3}]O_4$$

Here, M^{3+} is Bi^{3+} ions enclosed by round brackets correspond to tetrahedral (A) site and the ions enclosed by square brackets correspond to octahedral (B) site. This cation distribution is presented from the fact that Cd^{2+} is a non - magnetic ion and has strong preference for A - site. On the other hand, Co^{2+}, and Bi^{3+} have strong preference for B - site. The observed and calculated magnetic moment (n_B) was evaluated by using the relation given in the literature is listed in Table V. From Table V it can be immediately noticed that the substitution of Bi^{3+} lowers the values of M_S and n_B as compared to our previously reported values for unsubstituted $Cd_{1-x}Co_xFe_2O_4$ ferrites. In the present system the occupancy of Bi^{3+} on B site has expelled equal number of Fe^{3+} ions to A - site because of which the magnetic character is found to reduce. Though the values of M_S and n_B are lowered the nature of Cd concentration dependence remains the same. Therefore, what we discussed before remains true for Bi^{3+} substitution also, i.e. existence of Nèel's two - sublattice. It has been observed that in case of x = 1, the observed and calculated magnetic moments (n_B) are slightly less than the calculated ones. This small variation may be due to the preparative technique. The observed n_B values for $x \geq 0.4$ are lower than the calculated n_B values (Table V). These low magnetic moments can be explained in terms of the non - collinear spin arrangement i.e. the presence of a small canting of the B site moment with respect to a direction of the A site moment.

Table V: Magnetic properties and curie temperature (Tc) for $Cd_{1-x}Co_xFe_{1.7}Bi_{0.3}O_4$ systems ($0 \le x \le 1$)

Compounds	Coercive Force (Hc)± 0.50e	Saturation Magnetization (Ms) ± 2 emu g^{-1}	Ratio of M_R/M_S	Magnetic Moment $n_B \pm 0.1$ BM		Curie Temp.	$<\theta_{Y-K}>$ Angles Observed
				Observed	Calculated		
$Cd_{0.8}Co_{0.2}Fe_{1.7}Bi_{0.3}O_4$	375	24.55	0.35	1.421	10.246	528	74^o 39'
$Cd_{0.6}Co_{0.4}Fe_{1.7}Bi_{0.3}O_4$	215	62.85	0.22	3.518	8.562	563	59^o 9'
$Cd_{0.4}Co_{0.6}Fe_{1.7}Bi_{0.3}O_4$	275	79.14	0.24	4.269	7.058	606	27^o 57'
$Cd_{0.2}Co_{0.8}Fe_{1.7}Bi_{0.3}O_4$	675	72.48	0.52	3.780	5.464	672	4^o 11'
$CoFe_{1.7}Bi_{0.3}O_4$	425	72.73	0.57	3.653	3.870	740	0

The values of $<\theta_{Y-K}>$ calculated by above equation are presented in Table V. This value is zero for x = 1, while it is positive for other compositions. As can be noted from Table V, with increasing cobalt content (x) these $<\theta_{Y-K}>$ values are found to decrease. This is in conformity that Nèel's two sublattice model is dominant at higher concentration of cobalt and triangular spin arrangement becomes prominent at lower cobalt concentration, where $<\theta_{Y-K}>$ angles go on decreasing and finally become zero. Thus, the observed variation of the saturation magnetization (M_S) with cobalt concentration has been explained on the basis of the existence of Yafet - Kittel angles on the B - site spins.

The coercive force (H_C) and remanance ratio (M_R/M_S) for all compounds with $x \ge 0.2$ increases as cobalt content increases. This indicates that the magnetic behaviour of the system approaches that of a random system of non - interacting single domain particles with cubic symmetry.

Initial magnetic susceptibily

Figure 4 shows the temperature variation of initial magnetic susceptibily (χ_i) curves for $Cd_{1-x}Co_xFe_{1.7}Bi_{0.3}O_4$ with $x \ge 0.2$. For these compounds, χ_i increases with increasing temperature giving a broad peak value and then suddenly becomes zero just before the Curie temperature (Fig.4) i.e. called Hopkinson effect. This is a characteristic behaviour of compounds having a single domain grain. The curie temperature (T_C) for $x \ge 0.2$ compounds are determined from these curves and are listed in Table V. T_C values are found to increase with increasing cobalt concentration (x) at B - site, probably due to strengthening of the A - B interaction. The substitution of Bi^{3+} ion results in decrease of the Curie temperature as compared to our previously reported value for unsubstituted ferrites. This may be due to dilution in the Fe - Fe interactions on octahedral (B) site, because the Bi - Fe and Bi - Bi interactions are smaller than Fe - Fe interaction.

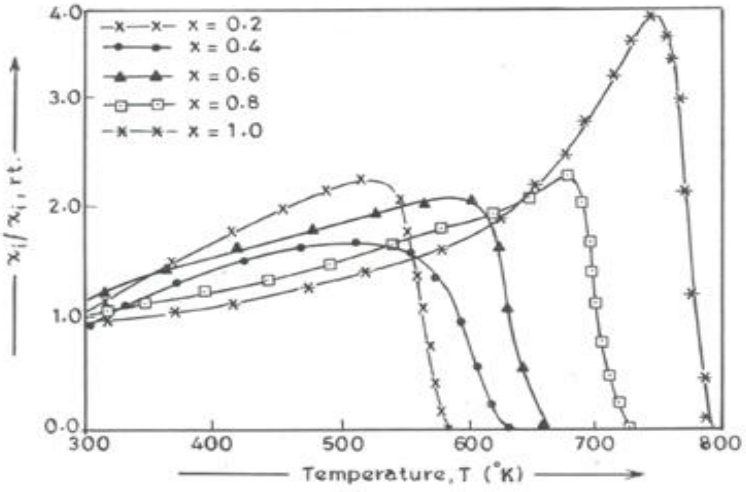

Fig. 4: Plot of χ_i/χ_i, r.t. against temperature (T) for the systems For $Cd_{1-x}Co_xFe_{1.7}Bi_{0.3}O_4$ systems ($0 \le x \le 1$).

CONCLUSIONS

X-ray powder diffraction patterns of $Cd_{1-x}Co_xFe_{1.7}Bi_{0.3}O_4$ compounds possess spinel structures. The lattice parameter decreases linearly with increase of cobalt concentration in these compounds. The particulate properties like X-ray density and apparent density decreases, while porosity increases as a function of cobalt concentrations (x) for these compounds. The mean crystallite size for all compounds did not show any trend as x increases. Temperature variation

of direct current electrical conductivity of $Cd_{1-x}Co_xFe_{1.7}Bi_{0.3}O_4$ show a definite kink except x = 0.0 and 0.2, which corresponds to ferrimagnetic to paramagnetic transitions. The activation energies (Ea) for electrical conduction were found to increase, while the conductivity (σ) decreases as the cobalt ion concentration increases. The thermoelectric power for all compounds is of negative over the while range of temperatures; indicating that the charge carriers are electrons. The compounds of the system $Cd_{1-x}Co_xFe_{1.7}Bi_{0.3}O_4$ with $x \geq 0.2$ showed a definite hystersis loop. The coercive force, saturation magnetization and remanance ratio (M_R/M_S) increases as cobalt content increases. The composition, for x = 0.0 to x = 0.2 have Y-K model prevails, while for x = 0.4 to 0.8 both Nèel's two sublattice model and Y-K model simultaneously exist. The temperature variation of initial magnetic susceptibility suggests that these samples have single domain grains. The Curie temperature is found to increase with increasing cobalt content.

REFERENCES

[1]. J. Khemprasit, S. Kaen-ngam, B. Khumpaitool, P. Kamkhou, J. Magn. Magn. Mater. 323, (2011) 2408.
[2]. Y.Q. Song, H.W. Zhang, Q.Y. Wen, Y.X. Li, J.Q. Xiao, Chin. Phys. Lett. 24, (2007) 218.
[3]. A.K.Nikumbh, R.A.Pawar, D.V.Nighot, G.S.GugaleM.D.Sangale, M.B.Khanvilkar and A.V.Nagawade, Journal of Magnetism and Magnetic Materials, 355 (2014) 201.
[4]. N.H. Jadhav, S.S. Sakate, N.K. Rasal, D.R. Shinde and R.A. Pawar, ACS omega, 4 (2019) 8522.
[5]. S.F. Shaikh, R.S. Mane, Y.J. Hawang, O.-S. Joo, Electrochim. Acta., 167, (2015) 379.
[6]. P. Sharma, A. Gupta, K.V. Rao, F.J. Owens, R. Sharma, R. Ahuja, J.M.O. Guillen, B. Johansson, G.A. Gehring, Nat. Mater., 2, (2003), 673.
[7]. D.P. Joseph, S. Naveenkumar, N. Sivakumar, C. Venkateswaran, Mater. Chem. Phys. 97, (2006) 188.
[8]. R.A. Pawar, A.K. Nikumbh, D.S. Bhange, N.J. Karale, D.V. Nighot, M.B. Khanvilkar, Bulletin of Materials Science, 40 (2017) 1335.
[9]. A.M. Abdel Hakeem, J. Magn. Magn. Mater. 324, (2012) 95.
[10]. B. Ali, L.R. Shah, C. Ni, J.Q. Xiao, S.I. Shah, J. Phys. Condens. Mater. 21, (2009) 456005.
[11]. M.B. Khanvilkar, A.K. Nikumbh, R.A. Pawar, N.J. Karale, D.V. Nighot, G. S. Gugale, Journal of Materials Science: Materials in Electronics, 30 (2019) 13217.
[12]. J. Massoudi, M. Smari, K. Nouri, E. Dhahri, K. Khirouni, S. Bertaina, L. Bessais and E. K. Hlilf, RSC Adv., 10 (2020) 34556.
[13]. Rajesh Iyer, Rucha Desai and R.V.Upadhyay, Indian J. Pure and Appl. Phys. 47 (2009) 180.
[14]. N.D.Patil, N.B.Velhal, N.L.Tarwar and Vijaya R.Puri, Int.J.Eng. and Innovative Tech. 3 (2014) 73.
[15]. S.P.Dalwai, T.J.Shinde, A.B.Gadkari and P.N.Vasambekar, Bull.Matter Sci.36 (2013) 919.
[16]. N.D.Patil, M.B.Shelar and V.Puri, Int.J.Self. High propogating High Temp. synthesis 21 (2012) 212.
[17]. S.A. Jadhav, S.B. Somvanshi and M.V. Khedkar, J Mater Sci: Mater Electron, 31, (2020) 11352.
[18]. Ombretta masala and Ram Seshadri, Annu Rev. matter Res. 34 (2004) 41
[19]. Xiao Xu Xian, Huang Kelong, Yan Jian Hui , H.E.Qiong , Trans. Nonferrous Met. Soc. China, 5 (2005) 1172.
[20]. Sivan Klas, Yael Dubowski, Ori Lahav, J.Hazardous Mat. 193 (2011) 59.
[21]. N.J. Karale-Unde, A.K. Nikumbh, M.B. Khanvilkar, P.A. Nagawade, R.A. Pawar, D.V. Nighot, S.B. Misal, G.S. Gugale, Journal of Materials Science: Materials in Electronics, (2021) 1.
[22]. A. B. Kulkarni and S. N. Mathad, Mat.Sci. for Energy Tech., 3, (2019), 455.
[23]. A. Vedrtnam, K. Kalauni, S. Dubey and A. Kumar. AIMS Materials Science, 7, (2020) 800.
[24]. A. Omelyanchik, K. Levada, S. Pshenichnikov, M. Abdolrahim, M. Baricic, A. Kapitunova, A. Galieva, S. Sukhikh, L. Astakhova, S. Antipov, B. Fabiano, D. Peddis and V. Rodionova, Materials, 13, (2020) 5014.
[25]. M. K. Anupama and B. Rudraswamy, IOP Conf. Ser.: Mater. Sci. Eng. 149, (2016) 12194.
[26]. S.M. Mane, P.M. Tirmali, S.L. Kadam, D.J. Salunkhe, C.B. Kolekar, S.B. Kulkarni, Advances in Applied Ceramics, 116 (2017) 325.
[27]. M. Kanwal, I. Ahmad, T. Mydan, Journal of Elec. Materi. 47, (2018) 5370.
[28]. A.K. Nikumbh, S.B. Misal, D.V. Nighot, P.A. Nagawade, N.J. Karale, A.S. Deshpande, G.S. Gugale, A.V. Nagawade, Journal of Alloys and Compounds, 683 (2016) 346.
[29]. S. Mane, P. Tirmali, S. Kadam, A. Tarale, C. Kolekar, S. Kulkarni, Journal of the Chinese Advanced Materials Society, 4 (2016) 269.
[30]. V. Pandit, S. Arbuj, Y. Pandit, S. Naik, S. Rane, U. Mulik, S. Gosavi, B. Kale, RSC Advances, 5 (2015) 10326.
[31]. V. Pandit, S. Arbuj, U. Mulik, B. Kale, Environmental science & technology, 48 (2014) 4178.
[32]. V. Pandit, S. Arbuj, R. Hawaldar, P. Kshirsagar, J. Ambekar, U. Mulik, S. Gosavi, B. Kale, RSC advances 5 (2015) 13715.
[33]. V. Pandit, S. Arbuj, R. Hawaldar, P. Kshirsagar, U. Mulik, S. Gosavi, C. Park, B. Kale, Journal of Materials Chemistry A, 3 (2015) 4338.
[34]. D. Kumbhar, V. Pandit, S. Deshmukh, J. Ambekar, S. Arbuj, S. Rane, Journal of Nanoengineering and Nanomanufacturing, 5 (2015) 227.
[35]. K. Nevase, S. Arbuj, V. Pandit, J. Ambekar, S. Rane, Journal of Nanoengineering and Nanomanufacturing 5 (2015) 221.
[36]. A. K. Nikumbh, A. V. Nagawade, V. B. Tadke and P. P. Bakare, J. Mater. Sci. 36 (2001) 653.